Applied Catalysis B: Environmental 184 (2016) 87–95

Contents lists available at ScienceDirect

Applied Catalysis B: Environmental

journal homepage: www.elsevier.com/locate/apcatb

Active Mn species well dispersed on Ca^{2+} enriched apatite for total oxidation of toluene

D. Chlala[a,b,c], J.-M. Giraudon[a,b,*], N. Nuns[a,d], C. Lancelot[a,b], Rose-Noëlle Vannier[a,e], M. Labaki[c], J.-F. Lamonier[a,b]

[a] Université Lille 59650, Villeneuve d'Ascq, France
[b] CNRS UMR 8181, Unité de Catalyse et Chimie du Solide, Cité Scientifique, Bâtiment C3, 59655, Villeneuve d'Ascq, France
[c] Lebanese University, Laboratory of Physical Chemistry of Materials (LCPM)/PR2N, Faculty of Sciences, Fanar, BP 90656, Jdeidet El Metn, Lebanon
[d] IMMCL Chevreul, Institut des Molécules et de la Matière Condensée, 59655, Villeneuve d'Ascq, France
[e] ENSCL, 59655, Villeneuve d'Ascq, France

ARTICLE INFO

Article history:
Received 24 June 2015
Received in revised form 8 November 2015
Accepted 16 November 2015
Available online 28 November 2015

Keywords:
Hydroxyapatite
Toluene abatement
ToF-SIMS
Manganese–calcium oxidized species

ABSTRACT

Hydroxyapatite (Hap)-supported manganese oxide catalysts (10 wt% Mn based on MnO_2) were prepared by two different routes, from Mn nitrate (Nit) and Mn acetate (Ac) precursors. The catalyst precursors were calcined at 400 °C for 4 h to get the final MnNit-Hap and MnAc-Hap catalysts. Elemental analysis, XRD, SEM, HRTEM, N_2 adsorption experiments, FT-IR, temperature programmed reduction (H_2-TPR), X-ray photoelectron spectroscopy (XPS) and ToF-SIMS characterization methods were used to identify the Mn species and their environment. The overall characterization studies indicated that the nature of the counter-ion played a significant role in the speciation and dispersion of manganese species in Hap although the Mn AOS in both cases is around 3. The nitrate Mn precursor allowed to get after calcination at 400 °C well dispersed and easily reduced active Mn^{n+} ($n+\geq 3$) oxidized species on a Ca^{2+} enriched hydroxyapatite surface, likely in a polymeric form or/and in small Mn_xO_y crystallites, while part of Mn in the form of Mn^{2+} ions incorporated into the Hap substituting Ca^{2+} at the apatite surface. By opposition the acetate Mn precursor primarily results in large Mn_3O_4 oxide nanocrystals along with an amorphous Mn_5O_8 phase and Hap incorporated Mn^{2+} ions.

The total oxidation of toluene was investigated on these new catalysts and the catalytic performances were compared to those of a reference 10 wt%Mn on alumina (Mn–Al). It is found that the nature of the support plays a significant role. Indeed the different AOS of Mn (about 3 for supported Hap; ≈4 for supported alumina catalyst) showed that the Mn active phases are different. The best performances were achieved on the MnNit-Hap catalyst with the complete conversion of toluene at 220 °C. The Mn oxidized species well dispersed on Ca^{2+} enriched apatite using a strong oxidizing counter-ion as NO_3^- in the Mn precursor were responsible for optimal toluene conversion. In that case it was found that the incorporation of part of NO_3^- in the hydroxyapatite promoted the surface Ca^{2+} enrichment of Hap by the incorporation of Mn^{2+} into the Hap support.

1. Introduction

The research of new catalytic materials requires available cheap and non-toxic components. In the field of total oxidation of volatile organic compounds (VOCs) one approach among others is to disperse and calcine a transition metal precursor whose metal is well known as being active for such type of reaction, on a convenient support. A new and original synthetic pathway may involve the dispersion of a Mn precursor as Mn is an easily reducible/oxidable element on hydroxyapatite, $Ca_{10}(PO_4)_6(OH)_2$ (Hap), which is a safe and non-toxic material. Additionally the morphology of Hap crystallite can be easily tuned. In this way it has been previously reported the synthesis of elongated crystallites of Hap which are mainly cleaved in such a way that Ca atoms are more exposed on the surface [1]. Hence possible incorporation of the active phase into Hap has to be taken into account as Hap is recognized for its ability to easily exchange calcium ions exposed on the surface at site I (coordinated by 9 oxygen ions) and site II (coordinated by five oxygen ions and one hydroxyl group). Additionally the OH^- groups located in the centre of Hap column or channel parallel to *c*-axis are

* Corresponding author at: Université Lille, 59650, Villeneuve d'Ascq, France.
E-mail address: jean-marc.giraudon@univ-lille1.fr (J.-M. Giraudon).

http://dx.doi.org/10.1016/j.apcatb.2015.11.020
0926-3373/

closely related with the reactivity of Hap material [2,3]. A previous recent work reported on efficient Mn-Hap catalysts for direct imine formation by oxidative coupling of alcohols and amines but mainly focused on the acido–basic properties of the catalysts [4]. Pioneering work in this field aiming to dope Hap with a Cu active phase has been very recently reported [5]. The hypothesis of 5 possible sites for Cu location has been proposed on the features of Hap structure and experimental results. Additionally it has been found that the Cu location and species can be adjusted owing to the method of preparation. In our case, the knowledge of the speciation of manganese in terms of the possible variable valences of Mn (e.g. +2, +3, +4) and of the nature of the Mn species in interaction with the support offer exciting challenges to tune the physical–chemical and catalytic properties of such catalysts.

In the present work, the wet impregnation has been adopted to disperse Mn (10 wt%) species on Hap. The main challenging task is to be able to determine the location and nature of Mn species taking into account that Hap flexible structure offers a wide range of possible cationic as well as anionic substitutions. Many analytical techniques have been applied for catalyst characterization. The total oxidation of toluene has been investigated on these new catalysts and their catalytic performances have been compared to those of a reference 10 wt% Mn on alumina. Toluene was chosen as VOC probe molecule, because it is a commonly used solvent and presents an important POCP (Photochemical Ozone Creation Potential). The differences in catalytic performances have been discussed in terms of the effects of the nature of the counter ion of the Mn(II) precursor, the dispersion and the reducibility of the Mn related phases.

2. Experimental

2.1. Synthesis of the Hap support and supported Mn catalysts

The Hap was synthesised from a previous experimental procedure [1] according to the equation:

$$10Ca(NO_3)_2 + 6(NH_4)H_2PO_4 + 14NH_4OH \rightarrow Ca_{10}(PO_4)_6(OH)_2 + 20NH_4NO_3 + 12H_2O \quad (1)$$

150 mL of an aqueous solution containing 0.0835 mole of $Ca(NO_3)_2{\cdot}4H_2O$ (Sigma–Aldrich, purity ≥ 99.9%) were added dropwise to 500 mL of a 0.05 mol of $(NH_4)H_2PO_4$ (Sigma–Aldrich, purity ≥ 98.0%) solution placed under stirring at 80 °C. The pH during synthesis was maintained at 10 by properly adding a 25% NH_4OH solution. The formed precipitate was filtered, washed with hot water, and dried in an oven at 80 °C before being calcined at 400 °C for 4 h. The Ca/P was found to be 1.60. The reference alumina support supplied by Alfa Aesar (γ-Al_2O_3, purity: 99.97%; S_{BET} = 72 m^2/g) was used as received.

The Mn-Hap (Mn: 10 wt%) was prepared by a wet impregnation procedure. Typically 3.4–3.7 g of Hap was added in 50 mL of the aqueous Mn precursor solution ($Mn(NO_3)_2{\cdot}4H_2O$, Sigma–Aldrich, purity: 97%, (0.16 M); $Mn(CH_3CO_2)_2{\cdot}4H_2O$, Prolabo, purity: 99%, (0.14 M)). The solvent of the resulting mixtures was removed under constant stirring at 60 °C in a rotary evaporator (rotational speed: 20 rotations/min) under 70 mbar of pressure. The solids were dried overnight at 80 °C before to be calcined at 400 °C for 4 h under air to get MnNit-Hap (NO_3^- precursor) and MnAc-Hap ($CH_3CO_2^-$ precursor) samples. γ-Al_2O_3 (1.6 g) supported MnO_x (Mn: 10 wt%) was prepared in a same experimental procedure described for Mn-Hap using an aqueous solution of $Mn(NO_3)_2{\cdot}4H_2O$ (50 mL, 7.1×10^{-2} M) to get finally the Mn–Al sample.

2.2. Characterization of the catalysts

2.2.1. Elemental analyses

Mn, Ca and P analyses were performed by inductively coupled plasma spectroscopy-optical emission spectroscopy (ICP-OES) on an Agilent Technologies 700 Series spectrometer. Analysis was carried out at the REALCAT platform (Lille University). Prior to the analysis about 20 mg of sample were dissolved into 50 mL of an aqua regia solution.

2.2.2. X-ray diffraction

Routine powder X-ray diffractograms were recorded at room temperature (RT) using a Bruker AXS D8 Advance diffractometer working in a Bragg–Brentano geometry and equipped with a Lynx Eye Super Speed detector. Data were collected using the Cu Kα line in the 10–50° 2θ range with a 0.02° 2θ step and a counting time of 10 s per step. The Fullprof Suite program was used for Rietveld refinement on the Hap and MnNit-Hap samples. The Thompson–Cox–Hastings pseudo-Voigt function was chosen for describing the peak profiles. LaB_6 was used as a standard to derive the instrument resolution. Here, an anisotropic size broadening model based on linear combination of spherical harmonics was used to simulate the size broadening, and 6 additional parameters were refined. From this refinement, the individual size of Hap crystallite was derived for each crystallographic plane. Additionally the mean crystallite size of the supported Mn oxides was calculated by the Scherrer equation for the other samples using LaB_6 as a standard to derive the instrument resolution.

2.2.3. Scanning electron microscopy

The morphology of the materials was observed using Scanning Electron Microscopy images recorded on a Hitachi S-4700 apparatus with a 20k magnification equipped with micro-analysis (Energy-Dispersive X-ray Spectroscopy, EDS).

2.2.4. Transmission electron microscopy

Transmission electron microscopy (TEM) images were taken on a TECNAI electron microscope operating at an accelerating voltage of 200 kV equipped with a LaB_6 crystal. Prior to TEM observations, samples were deposited from ethanolic solution onto holey-carbon copper grids.

2.2.5. N_2 adsorption experiments

The specific surface areas were determined using a conventional multipoint BET nitrogen adsorption method with a Micromeritics Tristar II apparatus. Prior to nitrogen adsorption, the samples were outgassed for 4 h at 200 °C under vacuum.

2.2.6. Fourier transform-infrared spectroscopy

Fourier-transform transmission infrared (FT-IR) spectra were recorded from 200 cm^{-1} to 4000 cm^{-1} at room temperature in a Nicolet 460 Fourier transform infrared spectrometer. The samples were prepared by intimately mixing 1 mg of powdered sample with 60 mg of dried KBr. The spectra were obtained with spectral resolution of 4 cm^{-1}. All FT-IR spectra were an average of 256 scans at a resolution of 4 cm^{-1}.

2.2.7. Temperature programmed reduction-mass spectrometry

Temperature programmed reduction (TPR) were carried out using a Micromeritics 2920 Autochem II Chemisorption Analyzer. All the experiments were performed in a U-shaped tubular quartz reactor coupled to a quadrupole mass spectrometer (Omnistar, Balzers). Before starting the H_2-TPR, the sample (fresh samples: 200 mg; used samples: 100 mg) was treated in flowing Ar at 150 °C for 60 min. After cooling in flowing Ar the H_2-TPR measurement

was performed in 5 vol.% H_2/Ar (50 mL min^{-1}) up to a temperature of 800 °C (10 °C min^{-1}).

Calibration of the TPR peaks was carried out by evaluating the amount of H_2 from the average peak area from five pulses of 5 vol.% H_2/Ar (50 mL min^{-1}) using a loop volume of 0.4 mL. The quantification of the amount of H_2 resulting from the transformation of NO_3^- into NO was performed from the knowledge of the amount of the production of NO. The determination of the peak (m/z = 30) area by mass-spectroscopy was carried out by integration. Comparison with a reference area derived from 5 pulse peaks of knowing compositions (5% NO/He; loop volume: 0.4 mL) allowed to determine the NO amount. The quantity of hydrogen required to reduce NO_3^- into NO, Y, was estimated from the Relation (1) taking into account the stoichiometry of the transformation:

$$Y = 1.5n_{NO} = 1.5n_{NO3-} \quad (1)$$

Hence, the amount of hydrogen reducing Mn^{n+} into Mn^{2+} was obtained by subtracting Y from $n_{H2,}$ the total amount of hydrogen consumed, estimated from peak integration of the TCD signal. The Average Oxidation State (AOS) of Mn was estimated according to the following equation:

$$AOS(Mn) = 2 + 2\left(\frac{n_{H_2}/g_{cat} - Y/g_{cat}}{n_{Mn}/g_{cat}}\right) \quad (2)$$

where g_{cat} was the weight of the catalyst and n_{Mn} the experimental Mn molar content determined by elemental analysis.

2.2.8. X-ray photoelectron spectroscopy

XPS experiments were performed using an AXIS Ultra DLD Kratos spectrometer equipped with a monochromatised aluminium source (Al Kα = 1486.7 eV) and charge compensation gun. All binding energies were referenced to the C 1 s core level at 285 eV. Simulation of the experimental photo-peaks was carried out using a mixed Gaussian/Lorentzian peak fit procedure according to the software supplied by CasaXPS. Semi-quantitative analysis accounted for a nonlinear Shirley background subtraction. The XPS quantification was performed from the study of peak core levels Ca 2p, P 2p, Mn 2p, C 1s, O 1s and N 1s.

2.2.9. Time of flight-secondary ion mass spectrometry

Positive and negative ToF-SIMS measurements were performed with a ToF-SIMS^5 spectrometer (ION-TOF GmbH Germany) equipped with a bismuth liquid metal ion gun (LMIG). The compacted samples were bombarded with pulsed Bi_3^+ primary ion beam (25 keV, 0.25 pA) rastered over a 500 × 500 μm^2 surface area. With a data acquisition of 100 s, the total fluence does not amount up to 10^{12} ions/cm^2 ensuring static conditions. Charge effects were compensated by means of a 20 eV pulsed electron flood gun. In these experiments the mass resolution (m/Δm) was about 3200 at m/z = 175 for Ca_2PO_4. The containing $Ca_xMn_yO_z^+$ fragments were identified by their exact mass, coupled with the appropriate intensities for the expected isotope pattern.

2.3. Catalytic tests

Catalytic oxidation runs for abatement of toluene were performed in a continuous flow fixed bed Pyrex micro-reactor at atmospheric pressure. About 0.2 g of catalyst was placed in the reactor for each run. The reactive gas mixture was 800 ppmv of toluene diluted in air (100 mL min^{-1}) corresponding to a Volume Hourly Space Velocity (VHSV) of 500 mL g^{-1} min^{-1}. Flow rate was adjusted and controlled with digital flowmeter (MFC Mass Flow Controller). The micro reactor was placed in an electrical furnace. All the lines were heated at 120 °C. Catalysts were evaluated in the temperature range of 390 °C—room temperature, with a rate decrease of 0.5 °C min^{-1}. Before each run, the samples were pretreated 2 h at 390 °C under air flow of 75 mL min^{-1}. The concentrations of the gaseous species exiting from the inlet and outlet gas stream were analyzed on line by Gas Chromatography (7860A Agilent Gas Chromatograph) equipped with a Thermal Conductivity Detector (TCD) and Flame Ionization Detector (FID) and with two columns: Restek Shin Carbon ST/Silco HP NOC 80/100 micro packed, to separate permanent gases (Air, CO and CO_2) and a capillary column Cp-Wax 52CB25 m, Ø = 0.25 mm, to separate hydrocarbons and aromatic compounds.

Toluene conversion (C_t) was calculated as follows:

$$C_t(\%) = \frac{[toluene]_i - [toluene]_t}{[toluene]_i} \times 100$$

where $[toluene]_i$ and $[toluene]_t$ were respectively toluene inlet and outlet concentrations.

Conversion to CO_2 was determined by:

$$C_{CO2}(\%) = \frac{[CO_2]_t \times 100}{7 \times [toluene]_i}$$

where $[CO_2]_t$ was the CO_2 outlet concentration.

The rate of toluene conversion was calculated owing to the formula:

$$r = \frac{F \times C_t}{n_{Mn}}$$

where r was the rate of toluene conversion expressed in mole of reacted toluene per mole of manganese and per hour. F was the flow rate of toluene in mole per hour and n the molar amount of manganese.

The apparent energy of activation of the catalysts and the associated pre-exponential factors were calculated assuming a first-order reaction rate with respect to toluene and zeroth order to O_2 (large excess) with a contact time (t) of 0.2 s for Mn10hap and 0.26 s for MnAl catalysts. These determinations were conducted for conversion of toluene kept below ca. 15% so that differential reaction conditions could be assumed, with negligible heat and mass-transfer effects. E the slope of the Arrhenius' plot was extracted from ln k_{APP} vs 1/T. For a supposed 1st-order reaction, k_{APP} is calculated from the conversion values as $k_{APP} = -\ln(1 - X)/\tau$ with X is the toluene conversion and τ is the residence time based on the catalyst volume [6].

For the duration test, the catalysts were pretreated 2 h at 300 °C (10 °C min^{-1}) in flowing air (75 mL min^{-1}) before to be cooled at 220 °C (10 °C min^{-1}). After 5 min of temperature stabilization, the duration test under 800 ppmv of toluene diluted in air (100 mL min^{-1}) was carried out for 40 h. The catalysts were labelled MnNit-HapU, MnAc-HapU and Mn–AlU.

3. Results and discussion

3.1. Structural, morphologic and textural characterizations

The elemental composition and textural properties of the Hap materials are shown in Table 1. The molar Ca/P ratio of 1.59–1.75 of the Mn-Hap samples agree with the Ca/P ratio of pure Hap and the Mn doped Hap have similar Mn loadings (10 wt% ± 1 wt%). The wide-angle XRD patterns of the materials are gathered in Fig. 1. XRD analyses only show the characteristic peaks of Hap for the MnNit-Hap catalyst. The non-observance of related Mn oxide phases over the surface of Hap indicates amorphous or/and well dispersed Mn oxidized species. By opposition the X-ray diffraction pattern of MnAc-Hap displays new peaks positioned at 2θ = 18.0° and 36.1° as well as an increase of the peak at 29.0° ascribed to the diffraction of the tetragonal phase Mn_3O_4 crystallites (hausmannite, PDF no. 00-024-0734) having a mean crystallite size of 26 nm. Regarding Mn–Al material it is found the presence of the pyrolusite phase

Table 1
Chemical composition and textural properties of the catalysts.

Sample	EA		d_c[a]	S_{BET} (m^2/g)		d_p[c]	V_p[d]
	Ca/P	Mn (wt%)	(nm)	Calcined	Used[b]	(nm)	(cm^3/g)
Hap	1.60	–	–	94	–	–	0.59
MnNit-Hap	1.59	11.0	–	76	73	55	0.38
MnAc-Hap	1.75	10.4	26	79	86	55	0.49
Mn–Al	–	10.3	17	75	71	64	0.31

[a] Crystallite size of Mn phase.
[b] After test of stability.
[c] d_p: BJH desorption maximum pore diameter.
[d] Pore volume.

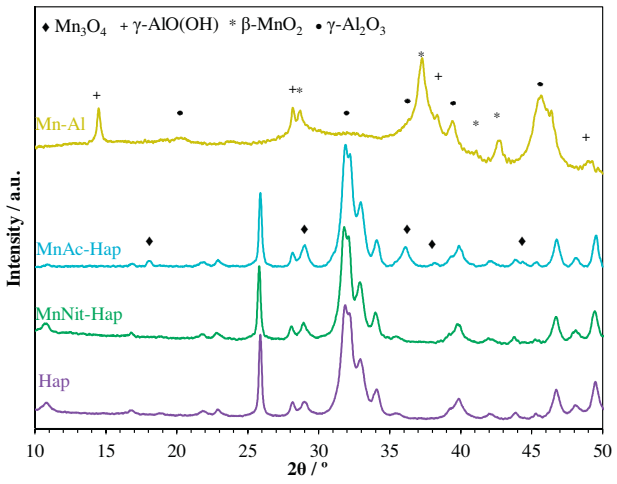

Fig. 1. XRD of the Hap support and supported Mn catalysts.

β-MnO_2 (PDF no. 00-024-0735) along with γ-Al_2O_3 (PDF no. 01-10-0425) and AlO(OH) (PDF no. 01-83-1505) phases. This is in line with previous studies showing that on alumina support β-MnO_2 is formed mainly below 430 °C [7–9]. The apatite structure was refined in the $P6_3/m$ space group, using the structure model proposed by Hughes et al. (Fig. S1) [10]. The calculated MnNit-Hap cell parameters $a = 9.4041(4)$ Å and $c = 6.8856(2)$ Å are close to those of Hap ($a = 9.4077(5)$ Å and $c = 6.8888(4)$ Å). The partial substitution of phosphate groups by carbonate was evaluated by refining the occupancy of phosphorous sites. It was found that the phosphorous occupancy (expressed in %) kept rather similar irrespective of Mn addition: 93.6(4) for Hap, 92.2(4) for MnNit-Hap suggesting the presence of a small amount of carbonates in the B-sites. Refinement of calcium sites led to calcium occupancy of 100% for Mn samples indicating no vacancies to be filled.

The crystallite size determined from the peaks relative to (1 0 0) and (0 0 1) planes, determined by Rietveld refinement using an anisotropic size-broadening model as previously reported [10] are 11 and 31 nm for Hap, 10 and 31 nm for MnNit-Hap. The length/thickness ratio of Hap determined from the ratio of the crystallite size along the (1 0 0) and (0 0 1) planes was 2.8 and slightly higher for MnNit-Hap (3.1) suggesting similar elongated crystallite shapes. The anisotropy observed by XRD was then confirmed by SEM (Fig. 2). Irregularly shaped agglomerates were observed for the Hap (Fig. 2a) while flat rods shaped clusters were observed for MnNit-Hap (Fig. 2b). It is worthwhile to mention that the corresponding Ca/P atomic ratio extracted from the EDS analyses of 1.89 and the Mn weight percentage of 13.4 (Fig. S2) agree with the expected values. Consistent with the aforementioned observations it was shown by TEM that the MnNit-Hap grains displayed rod-like morphology with a length of about 50 nm (Fig. 2c). The BET surface area of the Hap support was 94 $m^2\ g^{-1}$ and the pore volume was 0.59 $cm^3\ g^{-1}$. When adding Mn, the BET surface area values decrease from about 20% and 10% for MnNit-Hap and Mnac-Hap respectively. The nitrogen adsorption–desorption isotherms for Hap and Hap-supported Mn samples (not shown here) display the characteristic hysteresis loop of a Type IV isotherm (IUPAC) lying in the P/P_0 range of 0.7–0.99 exhibiting mesoporous character.

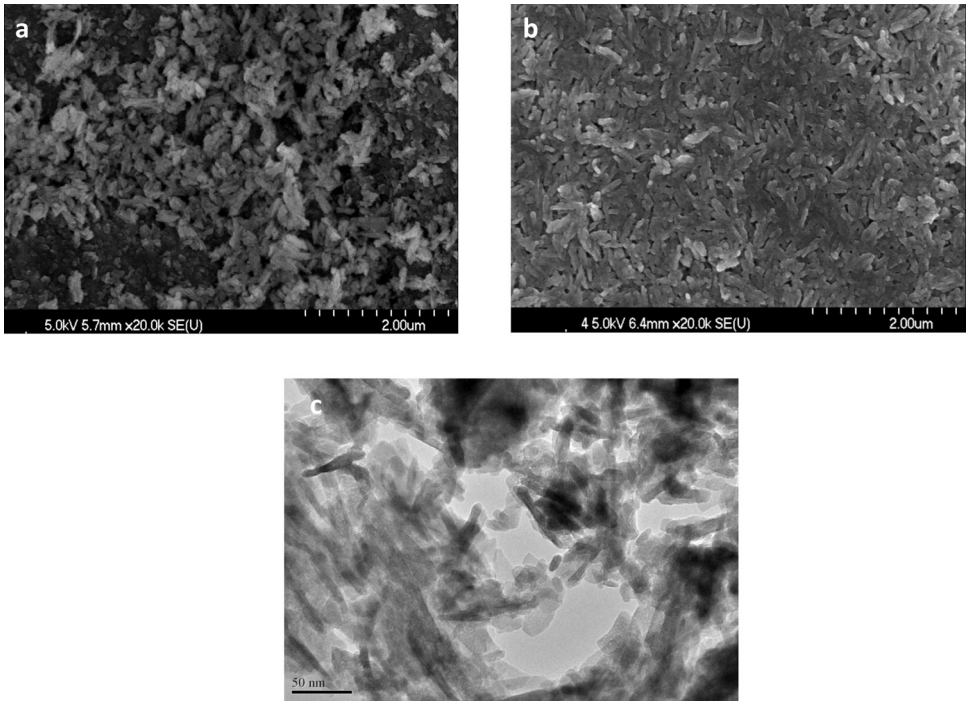

Fig. 2. SEM images of calcined samples at 200k magnification for (a) Hap; (b) MnNit-Hap; (c) TEM image of MnNit-Hap.

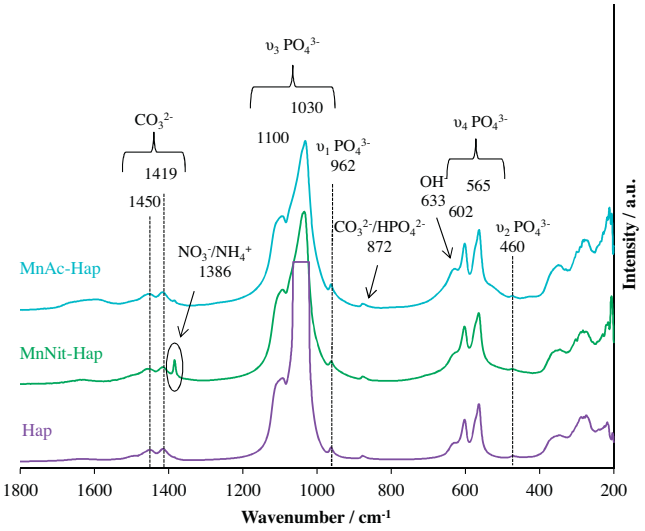

Fig. 3. FT-IR spectra of Hap and Hap supported Mn catalysts in the 200–1800 cm^{-1} window.

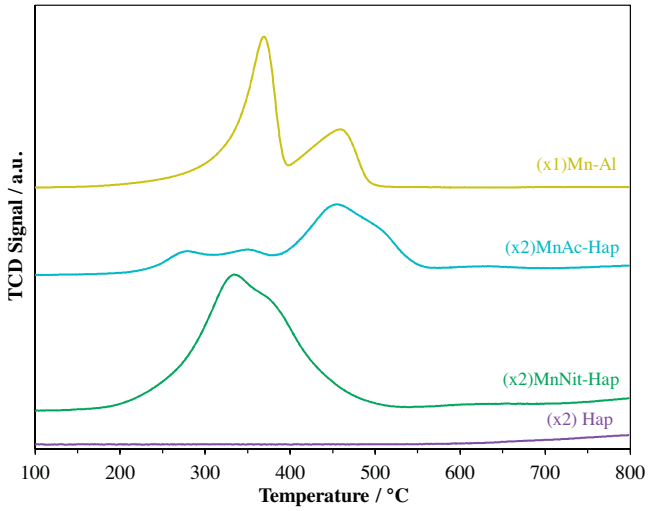

Fig. 4. H_2-TPR traces in function of temperature over the fresh supported Mn samples.

Table 2
Quantitative results from H_2-TPR and Mn AOS.

Catalysts	Consumed H_2 (mmol/g)	Desorbed NO (mmol/g)	Corrected consumed H_2 (mmol/g)	Mn AOS
MnNit-Hap	1.26	0.18	0.99	3.0
MnAc-Hap	0.65	–	0.65	2.7
Mn–Al	1.83	–	1.83	4.0
MnNit-HapU	0.49	–	0.49	2.5
MnAc-HapU	0.35	–	0.35	2.4
Mn–AlU	0.74	–	0.74	2.8

3.2. IR spectra of the Hap samples

Fig. 3 represents the 200–1800 cm^{-1} domain of the IR spectra of the related Hap samples. All the IR spectra confirmed the presence of carbonate-containing apatites with bands at 872 cm^{-1}, 1450 cm^{-1} and 1419 cm^{-1} [11–13]. The fundamental vibrational modes of PO_4 species gave rise to bands at 565 cm^{-1}, 602 cm^{-1}, 962 cm^{-1} and 1030–1100 cm^{-1}, as reported previously [14,15]. Further, HPO_4^{2-} groups might also be present, with the characteristic band at 872 cm^{-1}. However, this latter is known to overlap with a carbonate band, making straightforward conclusions impossible [11]. The presence of residual NO_3^- species is attested by the presence of a sharp nitrate band in the vicinity of 1385 cm^{-1} in the FT-IR pattern of the MnNit-Hap-Pre which is the sample MnNit-Hap prior calcination (Fig. S3) [12,13] due to NO_3^- acting as surface adsorbed species. After the calcination step this IR line significantly decreases in intensity but still remains accounting for the persistence of NO_3^-. It is noteworthy that the increase of the duration of the calcination step up to 10 h does not change significantly the relative intensity of the NO_3^- characteristic IR-band. That observation strongly suggests that part of NO_3^- incorporates into the hydroxyapatite in line with a recent study indicating the propensity of Mn^{2+} and NO_3^- to associate within the Hap crystal structure [16].

3.3. Temperature-programmed reduction (TPR-MS) analysis

The H_2-TPR profiles of the different samples are reported in Fig. 4 and the amounts of H_2 consumed are given in Table 2. The H_2-TPR trace of Mn–Al sample shows a two-step reduction process characteristic for the reduction process of MnO_2 involving the phase transition process as follows:

$$MnO_2 \rightarrow Mn_2O_3\,(Mn_3O_4) \rightarrow MnO$$

The hydrogen consumption in the low temperature region is approximately 2/3 of the total hydrogen consumption (1/3 in the high temperature region). These amounts fit well with the theoretical ones assuming the global reduction of MnO_2 (Mn Average Oxidation State (AOS) of 4.0) to MnO with Mn_3O_4 as intermediate [17,18]. Indeed the XRD pattern of the powder after H_2-TPR performed at 800 °C reveals two new reflections positioned at $2\theta = 34.8$ and 40.3° which indicate the formation of the manganosite (MnO) phase (PDF no. 01-075-1090).

The pure Hap only reveals an onset of H_2 consumption at 600 °C. By opposition the reduction of MnAc-Hap results in three overlapping peaks with T_{max} = 274 °C, 347 °C and 450 °C. The third peak having a shoulder at 500 °C being much larger than the first two peaks of equal H_2 consumption. The Mn AOS of 2.7 (see below) agrees with the reduction of Mn_3O_4 detected by XRD however the reduction of bulk Mn_3O_4 exhibited only one reduction peak in contradiction with the obtained complex hydrogen consumption trace. The possibility of reducible species coming from the reduction of the counter anion contributing to the hydrogen consumption has been ruled out by MS results which do not reveal the production of significant amount of released gas molecules. As a result Raman spectroscopy has been performed over this sample in order to characterize some adventitious Mn amorphous phase(s). The resulting Raman spectrum depicted in Fig. S4 show numerous peaks. It is found an intense peak at 651 cm^{-1} and two other smaller peaks at 310 and 365 cm^{-1} ascribed to Mn_3O_4. Other peaks have also been observed at 264, 427, 475, 537, 581 and 620 cm^{-1} and have been attributed to Mn_5O_8. Indeed the Mn_5O_8 structure allowed 18 Raman-active modes (10 A_g + 8 B_g) with an intense A_g mode at about 647 cm^{-1} which is drawn here in the most intense mode of vibration of Mn_3O_4 [19,20]. It is noteworthy that Mn_5O_8 has a mixed valence nature. It is composed of 2D octahedral sheets of $[Mn_3^{4+}O_8]^{4-}$ consisting of Mn^{4+} ions in the *bc* plane separated by Mn^{2+} layers. Hence the TPR trace can be interpreted by the overlay of the H_2 consumption due to Mn_5O_8 and Mn_3O_4 [17]. The first peaks being ascribed to the first successive reductions of Mn_5O_8 owing to:

$$Mn^{4+} \rightarrow Mn^{3+} \rightarrow Mn^{3+/2+} \quad (2)$$

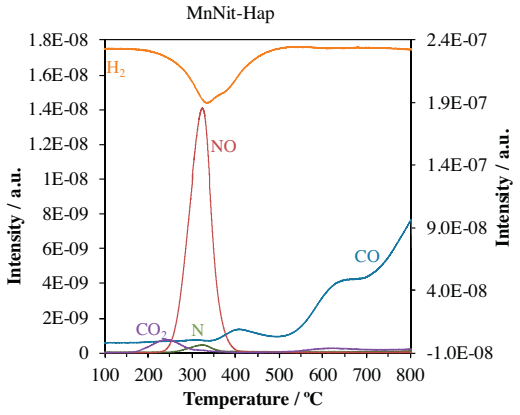

Fig. 5. Evolution of the $m/z = 2$, 28, 30 and 44 signals in function of temperature in TPR-MS experiment.

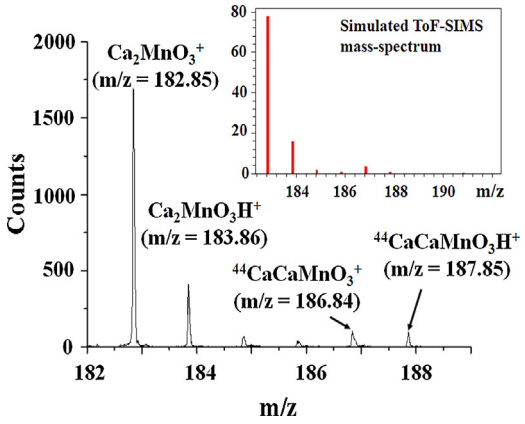

Fig. 6. ToF-SIMS mass spectrum of MnNit-Hap m/z: 182–189 range.

The last peak with the distinct shoulder is believed to be the convolution of two peaks resulting from the combined reduction of the Mn_3O_4 particles, initially still detected on the fresh sample and those originating from Mn_5O_8 partial reduction owing to Eq. (2), into MnO.

H_2-TPR profile of MnNit-Hap catalyst shows a broad intense reduction peak at temperature below 550 °C while a small very broad peak is observed at high temperature (HT > 550 °C). As residual NO_3^- coming from the Mn precursor and CO_3^{2-} incorporating in Hap are potential reductive species their release as gaseous species may contribute to the H_2 consumption. In order to check these possibilities the nature of the gaseous products produced in the course of the reductive treatment over MnNit-Hap has been monitored by mass spectrometry from the selected masses 30, 14 (NO); 44, 12 (CO_2), 28 (CO/N_2) and 44 (N_2O). The variations of the selected m/z signals as a function of temperature are gathered in Fig. 5. The $m/z = 2$ profile, which corresponds to hydrogen evolution, is very similar to the TCD trace. It is found that the H_2 consumption peak is partly related to the release of NO. Low productions of CO_2 (150–400 °C) and CO (from $T > 350$ °C) are also observed. However the CO formation resulting from the reduction of some CO_3^{2-} species do not contribute significantly to the global reduction process. Hence corrected hydrogen consumption relevant to MnO_x reduction has been evaluated taking into account the reduction process NO_3^- to NO for MnNit-Hap sample. A Mn AOS has been subsequently evaluated on the basis of the reduction of MnO_x into MnO as confirmed by XRD (Table 2). The Mn AOS of 3.0 for MnNit-Hap sample is higher than the Mn AOS for MnAc-Hap of 2.7 consistent with the oxidative character of the NO_3^- counter-ion. In terms of increasing reducibility, based on the temperature of onset of reduction, we can rank the catalysts as follows: Mn–Al < MnAc-Hap < MnNit-Hap.

3.4. XPS studies

XPS analysis has been then carried out to get surface information about the valence of Mn and its dispersion. Surface composition values from XPS data are listed in Table 3. The energy difference ΔE between the two lines of the Mn 3s core level has been used herein to get an XPS AOS of Mn. Indeed the average oxidation state of Mn increases linearly with the decrease of the Mn 3s doublet splitting energy owing to the formula $AOS = 8.956 - 1.13\Delta E$ as earlier reported by Galakhov et al. [21]. The XPS Mn AOS of 2.5–2.6 indicate a Mn mean valence between 2 and 3. The Ca/P ratios of 1.44 (1.46) were much lower than the bulk ratios of 1.59 (1.75) using Nit (Ac) respectively. Hence Ca species are less exposed to the surface than phosphates at least within the ca. 10 nm analysis depth limit of the XPS technique. Additionally the surface Ca/P ratio keeps constant with the nature of the counter-anion of the Mn precursor. However it has been reported recently that despite the observance of $(Ca/P)_{XPS} < (Ca/P)_{ICP}$, the Ca ions and O ions are more exposed to the first atomic layer of hydroxyapatites based on LEIS measurements [1]. It has been deduced that the apatite crystallites are mainly cleaved in such a way that Ca^{2+} present in ac and bc unit cell faces of apatite become more exposed to the surface if crystallite grows along the [001] direction [22,23]. The XPS spectra of the N 1s regions show typically 2 peaks positioned at 399.8 and 407.5 eV originating from the nitrate precursor. The high BE peak has been assigned to nitrate ion (NO_3^-) [24] while the peak at about 400 eV belongs likely to adsorbed NH_x [25]. The Mn dispersion increases substantially when moving from acetate to nitrate counter-ion. Indeed the XPS Mn/(Ca + P) ratio increases by ca. 50% for MnNit-Hap compared to MnAc-Hap showing the beneficial role of using a strong oxidizing counter-ion in the Mn precursor to enhance manganese dispersion.

3.5. ToF-SIMS study

To get insights into the elemental composition in the outermost atomic layers of solids, ToF-SIMS, a very sensitive technique, has been used. Due to its high sensitivity (study of trace levels up to 1 ppm) ToF-SIMS is able, contrarily to XPS, to give molecular information about surface and interfaces of the samples through the detection of molecular ions. Regarding the Hap support it is found in the negative spectrum the characteristic peaks shown include O^-, OH^-, P^-, O_2^-, PO^-, PO_2^-, and PO_3^-. Hence the fragment ions of PO_4^{3-} anion: P^- ($m/z = 31$), PO^- ($m/z = 47$), PO_2^- ($m/z = 63$), and PO_3^- ($m/z = 79$) are clearly observed. The characteristic peaks shown in the positive spectrum include (ion, m/z value): Ca^+, 40.0; CaO^+, 56.0; $CaOH^+$, 57.0 and Ca_2O^+, 96.0. It is also detected some impurities such as Na^+, Mg^+, K^+, and hydrocarbons. Several fragment ions were found to be derived from a $Ca_{10}(PO_4)_6(OH)_2$ precursor species (ion, m/z value) such as Ca^+, 39.96; $Ca_2PO_3^+$, 158.5; $Ca_2PO_4^+$, 174.4; $Ca_3P_2O_3H^+$,230.9; $Ca_4P_2O_4H^+$, 286.9; $Ca_5P_2O_5H^+$, 343.0; $Ca_6P_3O_4H_2^+$, 399.0. Subtraction of the hydroxyl ion OH^- from $Ca_5(PO_4)_3OH$ affords the ion $Ca_5(PO_4)_3^+$, 484.0. The ToF-SIMS (+) spectra of the MnNit-Hap and MnAc-Hap samples clearly identify $Ca_xMn_yO_z^+$ ions of significant intensity such as typically $CaMnO_2^+$, $Ca_2MnO_3^+$ and $Ca_2MnO_2^+$ (Fig. 6; Table 4). The total relative intensity (based on the total sum of the intensity of unsaturated ions) of calcium–manganese containing fragments amounts to 9.1 and 3.6% for MnNit-Hap and MnAc-Hap respectively. The high concentration of $Ca_xMn_yO_z^+$ ions for MnNit-Hap is related to the good dispersion of the calcium–manganese oxide related phases. At the opposite the

Table 3
XPS results of the Hap supported Mn catalysts.

Catalyst	ΔE (Mn3s)/eV	Mn AOS	Ca/P	Mn/Ca	Mn/P	Mn/(Ca + P)	N/Ca	C/Ca	O/Ca
MnNit-Hap	5.60	2.6	1.44	0.25	0.36	0.15	0.08	4.51	3.81
MnAc-Hap	5.75	2.5	1.46	0.16	0.24	0.098	–	1.60	3.14
MnNit-HapU	5.73	2.5	1.38	0.38	0.53	0.22	–	6.56	4.24
MnAc-HapU	5.76	2.5	1.65	0.18	0.29	0.11	–	3.12	3.60

Table 4
Relative intensity of the $Ca_xMn_yO_z^+$ ions detected by ToF-SIMS for the MnNit-Hap and MnAc-Hap before and after catalytic duration test.

$Ca_xMn_yO_zH_w$	MnNit-Hap ($/10^{-3}$)	MnNit-HapU ($/10^{-3}$)	MnAc-Hap ($/10^{-3}$)	MnAc-HapU ($/10^{-3}$)
CaMnO	17.66	28.93	7.520	14.08
$CaMnO_2$	28.58	30.35	9.908	12.72
$CaMnO_2H$	17.99	20.20	7.297	10.27
$CaMn_2O_3$	3.628	3.396	1.160	0.890
$CaMn_2O_3H$	1.835	2.268	0.718	0.892
$CaMn_3O_4$	0.848	0.877	0.374	0.246
Ca_2MnO_2	2.700	4.398	1.543	3.190
Ca_2MnO_3	13.22	15.10	5.650	8.261
Ca_2MnO_3H	3.067	3.712	1.571	3.233
$Ca_2Mn_2O_4$	1.097	1.282	0.321	0.271
Sum	90.65	110.5	36.07	54.08

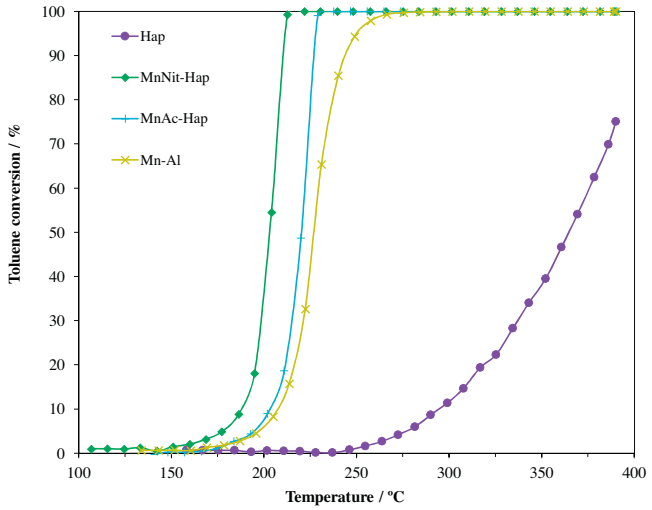

Fig. 7. Toluene conversion over the catalysts (GHSV = 30,000 mL h^{-1} g^{-1}; 800 ppmv toluene in air).

lower concentration of such ions for MnAc-Hap is linked to a lower Mn dispersion on the support and the crystalline character of the MnO_x phase in agreement with X-ray diffraction results showing the formation of Mn_3O_4 crystallites. The ToF-SIMS (−) spectrum exhibits the most intense Mn ions such as MnO_2H^-, MnO_3^- and MnO_3H^- in the m/z 2–150 range. Additionally the NO^-, 30.0; NO_2^-, 46.0 and NO_3^-, 62.0 ions are clearly observed on the MnNit-Hap sample and have been assigned to the presence of residual NO_3^- in agreement with previous results.

3.6. Catalytic tests

The toluene conversion in function of temperature is given over the different catalysts in Fig. 7. The complete oxidation of toluene is achieved for Mn based catalysts at temperatures below 270 °C while at 390 °C the conversion is only 75% for Hap. The addition of Mn remarkably enhances the toluene conversion. The toluene conversion based on T_{50} (°C) increases as follows: Hap (365) < Mn–Al (227) < MnAc-Hap (220) < MnNit-Hap (203). The corresponding rate of toluene conversion given at 203 °C expressed from the amount of Mn (Table 5) gives the similar order of increasing activity (in mol mol^{-1} Mn h^{-1}): Mn–Al (0.042) < MnAc-Hap (0.052) < MnNit-Hap (0.245). Hence there is evidence that the activity of the supported manganese species is dependent on the type of support and on the nature of the counter-ion of the manganese precursor for Hap support.

The differences found in activities may be partly explained by the variations in the nature and in the dispersion of the active Mn entities although the conjugation of other different factors like porosity, chemical nature, acidity, hydrophilic/hydrophobic balance of the support, manganese loading, may play a role. Regarding the acidity, the Mn–Al catalyst as expected appears more acidic than the Mn-Hap catalyst as previously reported in a previous study [4].

The Mn AOS decreases from 4 to 3 (or less) when moving from Al_2O_3 to Hap. This finding strongly suggests that the nature of the active phase changes with the support. It is expected in any case that the valence IV of manganese will be stabilize owing to the experimental conditions of the calcination in line with the observance of MnO_2 crystallites on alumina. Considering the Hap support the lower AOS of Mn can be explain by the easy substitution of Ca^{2+} surface sites by Mn^{2+}. The presence of this Hap incorporated Mn^{2+} ion has been herein evidenced by ESR study (not shown here) but the quantification is unfortunately impossible. The surface nature of the Ca^{2+} sites of the Hap directly involved in the Ca^{2+}–Mn^{2+} substitution may account for the none observance of vacancies to be filled at the calcium sites by Mn^{2+} when using XRD measurements which is a bulk characterization. Hence part of the amount of manganese is trapped as Mn^{2+} in the Hap structure. Afterwards the manganese dispersion on the Hap surface may occur. The nature of the oxidized Mn species is depending on the nature of the counter anion. When using acetate it is found large Mn_2O_3 crystallites in equilibrium with an amorphous Mn_5O_8 phase. By opposition when using nitrate anion it is found manganese in a polymeric oxidized form or/and in small Mn_xO_y crystallites, well dispersed on a Ca^{2+} enriched apatite. In both cases, anyway, it is detected a proportion of reduced Mn in the form of Mn^{2+} ions, mainly substituting Ca^{2+} sites at the apatite surface. Hence when regarding the Hap support competitive reactions may occur involving the diffusion of manganese into the support mainly as Mn^{2+} on the one hand and the interaction of Mn^{n+} with the Hap surface on the other. Such a diffusion process is believed to enrich the outermost layers of the apatite surface with Ca^{2+}. Additionally when using NO_3^- as counter-anion it has been clearly outlined that part of NO_3^- is trapped in the Hap structure minimizing the relative amount of this oxidant to play a role in the oxidation process of the manganese species in the course of the calcination step. Although the Mn AOS is rather similar for the two Hap related catalysts, it must be stressed that the speciation of Mn can be rather different, that is the relative distribution between the Mn(II), Mn(III) and Mn(IV) can change although the Mn AOS is the same.

Thus the better activity achieved on MnNit-Hap is supposed to be linked to the presence of well dispersed Mn species on Ca^{2+} enriched apatite enabling an enhanced toluene total oxidation. It

Table 5
Catalytic performances of the catalysts.

Catalysts	T_{50} (°C)	T_{90} (°C)	r (mol h^{-1} mol^{-1} Mn) at 203 °C	E_a (kcal mol^{-1})	LnA
MnNit-Hap	203	210	0.245	17	18
MnAc-Hap	220	227	0.052	33	35
Mn-Al	227	244	0.042	20	20

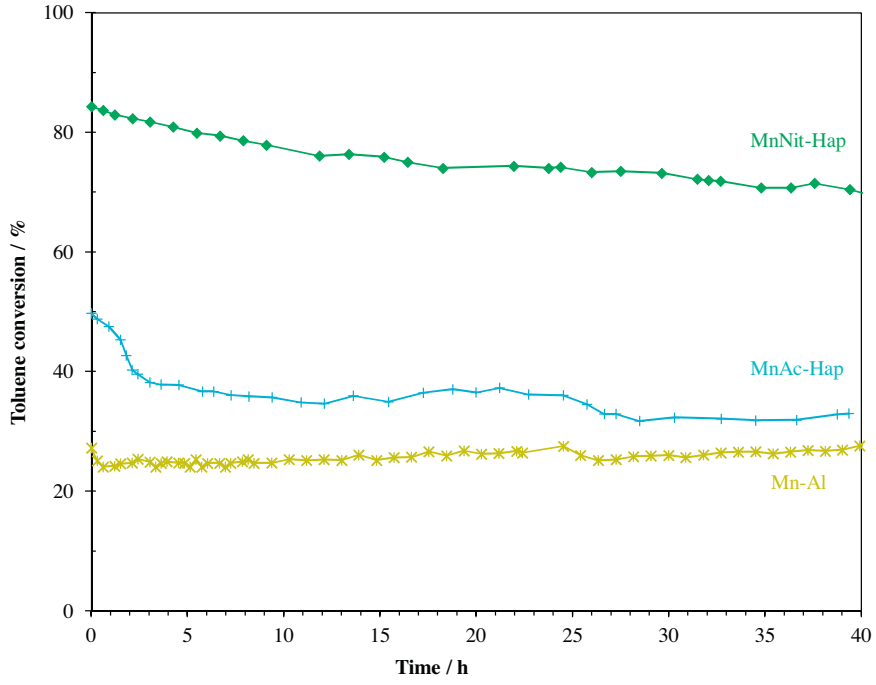

Fig. 8. Duration test performed at 220 °C over the supported Mn catalysts.

should be pointed out that the beneficial role of adding Ca^{2+} to bulk manganese oxides has already been reported in the literature [26].

The apparent activation energies given in Table 5 are in the range of those found in the literature [27]. The apparent activation energy over MnNit-Hap is two times lower to the one over MnAc-Hap. However it is found an inverse result when comparing the natural logarithms of the pre-exponential factor. Hence the nature of the counter-ion affects both E_a and the pre-exponential factor. Noteworthy the reactivity for toluene oxidation is correlated with the reducibility of the surface manganese oxide species in line with a redox mechanism as substantiate by previous results [28].

Toluene conversion in function of temperature into CO_2 is illustrated in Fig. S5. The ranking of the catalysts from T_{50CO2} (temperature at which 50% of the toluene is converted into CO_2) keeps unchanged. However it is noteworthy to mention that trace amounts of benzene and benzaldehyde are also detected in the course of the reaction besides CO and CO_2 formations. The CO production increases owing the sequence: MnAl < MnNit-Hap < MnAc-Hap (Fig. S6). However, at 100% toluene conversion, CO_2 appears as the sole carbon product of the reaction.

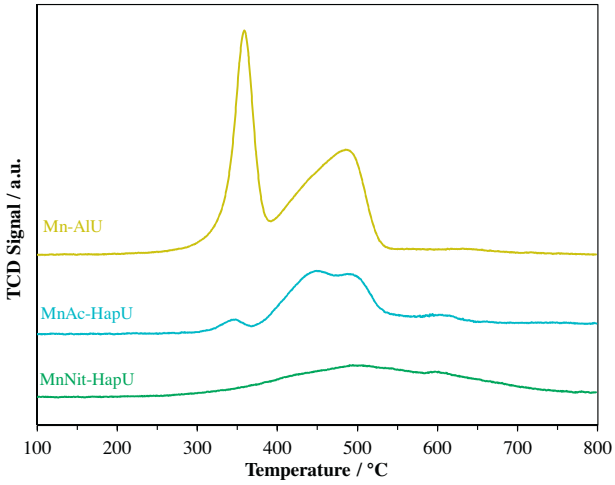

Fig. 9. H_2-TPR traces in function of temperature over the used supported Mn samples.

3.7. Durability tests

To demonstrate the potential industrial applicability, the catalysts have been involved in a long-run testing at 220 °C corresponding to toluene conversion of 90–20%, vs time for almost 40 h (Fig. 8). The MnNit-Hap catalyst deactivates slowly with time while the activity of MnAc-Hap keeps constant after initial deactivation. By opposition the activity of the Mn–Al catalyst is stable in the course of the reaction. The XRD pattern of the used Mn–Al sample (Mn–AlU; see Fig. S7) reveals new peaks at $2\theta = 36.1$ and 32.3° indexed to Mn_3O_4 (JCPDS: 00-024-0734; mean crystallite size: 27 nm) along those of the β-MnO_2 phase supported on alumina indicating a partial reduction of the catalyst.

The TPR trace of Mn–AlU shown in Fig. 9 results again in two peaks: P_1 and P_2 at 360 °C and 484 °C respectively with a hydrogen consumption ratio P_1/P_2 of 0.78. The P_1 peak is consistent with the reduction of MnO_2 into Mn_3O_4 followed by a reduction to MnO (part of P_2). The one reduction peak of Mn_3O_4 into MnO for its part

is drawn in the P_2 peak. Accordingly it is found a decrease of the total amount of the H_2 consumption per gram of catalyst during the TPR experiments by a factor of 2.5. This results in a decrease of the Mn AOS from 4.0 to 2.8.

On opposition no new crystalline Mn related phases are detected on Hap by XRD (Fig. S7). Regarding the reducibility of the samples, the TPR trace of MnAc-HapU differs from the initial one by the disappearance of the first low temperature peak ascribed to the reduction of Mn(IV) species to get a final Mn AOS of 2.4. The TPR profile of the MnNit-HapU sample in turn exhibits a broad flat envelope in the 300–750 °C temperature range having a maximum around 500 °C. It is also found a decrease of the Mn AOS from 3.0 to 2.5. Hence whatever the nature of the support and the Mn precursor reduction of the MnO_x related phases by the VOC/air mixture take place in the course of the reaction.

The XPS chemical composition of the used Hap supported Mn samples (sampleU) is given in Table 3. The splitting of the two peaks of the Mn 3s core-level spectra leads to a Mn AOS of 2.5 for Mn-HapU in agreement with the TPR results. The Ca/P ratio of 1.38 is close to the one reported earlier on the fresh sample of 1.44 (NO_3^- related samples) while the Ca/P ratio increases from 1.46 to 1.65 (Acetate related samples). Noteworthy the corresponding Mn/Ca and Mn/P ratios increase suggesting more Mn species exposed to the surface within 10 nm analysis. It is also found an increase in the C/Ca and O/Ca ratios which may be the result of adsorbed carbonaceous entities on Hap surface. ToF-SIMS results given in Table 4 show that the total relative intensity of calcium-manganese containing fragments amounts now to 11% and 5.4% for MnNit-HapU and MnAc-HapU respectively. These values are of the same order of those reported on the fresh catalysts in line with the rather good behavior of the catalysts with time on stream.

4. Conclusion

The hydroxyapatite Hap allows to get well dispersed Mn oxidized phases active for toluene oxidation using the Mn(II) nitrate precursor. While the AOS of Mn is close to 4 in Mn–Al, the AOS of Mn on hydroxyapatite decreases to 3. This is explained by the occurrence of competitive reactions involving the diffusion of manganese into the support mainly as Mn^{2+} on the one hand and the interaction of Mn^{n+} ($n \geq 3$) with the Hap surface on the other. The incorporation of some NO_3^- into the hydroxyapatite by the substitution of Ca^{2+} surface site by Mn^{2+} promotes the Ca^{2+} enrichment of the Hap surface and allows to maintain a good dispersion of the Mn^{n+} ($n \geq 3$) species contrarily to the Mn(II) acetate precursor. The manganese active phases are likely in the forms of Mn oxidized species, presumably in a polymeric form or/and in small Mn_xO_y crystallites taking advantage of Ca–O–Mn interactions with the support.

Acknowledgements

This research has been partially supported by the Nord-Pas de Calais Region in France through the Institute of Research in Industrial Environment (IRENI) project and by a French-Lebanese research project (PHC FL no. 32933QE).

The Fonds Européen de Développement Régional (FEDER), CNRS, Région Nord-Pas de Calais and Ministère de l'Education Nationale de l'Enseignement Supérieur et de la Recherche are acknowledged for fundings of X-ray diffractometers and XPS/LEIS/ToF-SIMS spectrometers within the Pôle Régional d'Analyse de Surface. Mrs. D. CHLALA acknowledges the award of a doctoral fellowship by the Agence Universitaire de la Francophonie (AUF) – Région du Moyen-Orient. The authors are grateful in particular to Olivier Gardoll (Lille University, France) for the TPR analyses, Martine Trentesaux for XPS analysis, Nora Djelal for SEM measurements and Laurence Burylo for XRD measurements.

Appendix A. Supplementary data

Supplementary data associated with this article can be found, in the online version, at http://dx.doi.org/10.1016/j.apcatb.2015.11.020.

References

[1] L. Silvester, J.-F. Lamonier, R.-N. Vannier, C. Lamonier, M. Capron, A.-S. Mamede, F. Pourpoint, A. Gervasini, F. Dumeignil, J. Mater. Chem. A 2 (2014) 11073.
[2] J. Suntivich, H.A. Gasteiger, N. Yabuuchi, H. Nakanishi, J.B. Goodenough, Y. Shao-Horn, Nat. Chem. 3 (2011) 546.
[3] M.I. Kay, R.A. Young, A.S. Posner, Nature 204 (1964) 1050.
[4] B. Chen, J. Li, W. Dai, L. Wang, S. Gao, Green Chem. 16 (2014) 3328.
[5] Z. Qu, Y. Sun, D. Chen, Y. Wang, J. Mol. Catal. A Chem. 393 (2014) 182.
[6] F. Duprat, Chem. Eng. Sci. 57 (2002) 901.
[7] A.K.H. Nohman, D. Duprez, C. Kappenstein, S.A.A. Mansour, M.I. Zaki, in: G. Poncelet, P.A. Jacobs, P. Grange, B. Demon (Eds.), Preparation of Catalysts V, Elsevier, Amsterdam, 1991, p. p 617.
[8] B.R. Strohmeier, D.M. Hercules, J. Phys. Chem. 88 (1984) 4922.
[9] P.W. Selwood, T.E. Moore, M. Ellis, J. Am. Chem. Soc. 71 (1949) 693.
[10] J.M. Hughes, M. Cameron, K.D. Crowley, Am. Mineral. 74 (1989) 870.
[11] N. Elazari, A. Ezzamarty, J. Leglise, L.C. de Ménorval, C. Moreau, Appl. Catal. A 267 (2004) 235.
[12] S. Kannan, I.A.F. Lemos, J.H.G. Rocha, J.M.F. Ferreira, J. Solid State Chem. 178 (2005) 3190.
[13] M.E. Fleet, X. Liu, Biomaterials 28 (2007) 916.
[14] G. Bonel, Ann. Chim. 7 (1972) 65.
[15] J.C. Elliott, J. Appl. Crystallogr. 13 (1980) 618.
[16] M. Gafurov, T. Biktagirov, G. Mamin, E. Klimashina, V. Putlayev, L. Kuznetsovac, S. Orlinskii, Phys. Chem. Chem. Phys. 17 (2015) 20331.
[17] F. Kapteijn, L. Singoredjo, A. Andreini, J.A. Moulijn, Appl. Catal. B Environ. 3 (1994) 173.
[18] R. Averlant, S. Royer, J.-M. Giraudon, J.-P. Bellat, I. Bezverkhyy, G. Weber, J.-F. Lamonier, Chem. Cat. Chem. 6 (2014) 152.
[19] C.B. Azzonia, M.C. Mozzati, P. Galinetto, A. Paleari, V. Massarotti, D. Capsoni, M. Bini, Solid State Commun. 112 (1999) 375–378.
[20] T. Gao, P. l Norby, F. Krumeich, H. Okamoto, R. Nesper, H. Fjellvåg, J. Phys. Chem. C 114 (2010) 922.
[21] V.R. Galakhov, M. Demeter, S. Bartkowski, M. Neumann, N.A. Ovechkina, E.Z. Kurmaev, N.I. Lobachevskaya, M.Ya. Mukovskii, J. Mitchell, D.L. Ederer, Phys. Rev. B 65 (2002) 113102.
[22] N.S. Resende, M. Nele, V.M.M. Salim, Thermochim. Acta 451 (2006) 16.
[23] T. Kawasaki, S. Takahashi, K. Ikeda, Eur. J. Biochem. 152 (1985) 361.
[24] J. Baltrusaitis, P.M. Jayaweeraac, V.H. Grassian, Phys. Chem. Chem. Phys. 11 (2009) 8295.
[25] Z. Zhou, Y. Huang, JPCS 188 (2009) 012033.
[26] S. Kim, W. Shim, Appl. Catal. B Environ. 98 (2010) 180.
[27] S.M. Saqer, D.I. Kondarides, X.E. Verykios, Appl. Catal. B 103 (2011) 275.
[28] F.N. Aguero, A. Scian, B.P. Barbero, L.E. Cadu, Catal. Lett. 128 (2009) 268.